ADVANCED HEALTHCARE MATERIALS
www.advhealthmat.de

Bone Morphogenetic Protein-2 Promotes Human Mesenchymal Stem Cell Survival and Resultant Bone Formation When Entrapped in Photocrosslinked Alginate Hydrogels

*Steve S. Ho, Nina L. Vollmer, Motasem I. Refaat, Oju Jeon, Eben Alsberg, Mark A. Lee, and J. Kent Leach**

There is a substantial need to prolong cell persistence and enhance functionality in situ to enhance cell-based tissue repair. Bone morphogenetic protein-2 (BMP-2) is often used at high concentrations for osteogenic differentiation of mesenchymal stem cells (MSCs) but can induce apoptosis. Biomaterials facilitate the delivery of lower doses of BMP-2, reducing side effects and localizing materials at target sites. Photocrosslinked alginate hydrogels (PAHs) can deliver osteogenic materials to irregular-sized bone defects, providing improved control over material degradation compared to ionically crosslinked hydrogels. It is hypothesized that the delivery of MSCs and BMP-2 from a PAH increases cell persistence by reducing apoptosis, while promoting osteogenic differentiation and enhancing bone formation compared to MSCs in PAHs without BMP-2. BMP-2 significantly decreases apoptosis and enhances survival of photoencapsulated MSCs, while simultaneously promoting osteogenic differentiation in vitro. Bioluminescence imaging reveals increased MSC survival when implanted in BMP-2 PAHs. Bone defects treated with MSCs in BMP-2 PAHs demonstrate 100% union as early as 8 weeks and significantly higher bone volumes at 12 weeks, while defects with MSC-entrapped PAHs alone do not fully bridge. This study demonstrates that transplantation of MSCs with BMP-2 in PAHs achieves robust bone healing, providing a promising platform for bone repair.

S. S. Ho, Dr. N. L. Vollmer, Prof. J. K. Leach
Department of Biomedical Engineering
University of California
Davis 451 Health Sciences Drive
Davis, CA 95616, USA
E-mail: jkleach@ucdavis.edu
Dr. M. I. Refaat, Prof. Dr. M. A. Lee, Prof. J. K. Leach
Department of Orthopaedic Surgery
School of Medicine
University of California
Davis, Sacramento, CA 95817, USA
Dr. O. Jeon, Prof. E. Alsberg
Department of Biomedical Engineering
Case Western Reserve University
Cleveland, OH 44106, USA
Prof. E. Alsberg
Department of Orthopaedic Surgery
Case Western Reserve University
Cleveland, OH 44106, USA

DOI: 10.1002/adhm.201600461

1. Introduction

Autologous bone grafting represents the gold standard for treatment of bone defects due to its osteoconductive, osteoinductive, and osteogenic nature.[1] Despite its safety and effectiveness, bone graft harvesting results in donor site pain and inflammation. There is a limited quantity of donor tissue available,[2] necessitating strategies that eliminate the need for autologous bone grafts. Cell-based approaches utilizing mesenchymal stem cells (MSCs) are under investigation for bone repair of atrophic nonunions, craniomaxillofacial defect repair, and hard palate reconstruction.[3] MSCs are multipotent cells that, among other phenotypes, can participate in bone formation directly by differentiating toward the osteoblastic phenotype[4–6] or indirectly by secreting paracrine acting trophic factors that stimulate angiogenesis and regulate local inflammation.[7–10] Regardless of their contribution, long-term survival and engraftment of MSCs to defect sites is poor,[11,12] drastically decreasing the therapeutic potential of MSC-based treatments. Strategies that boost cell retention will likely translate into greater functional benefit, motivating the need for improved methods to retain cells at the defect site while promoting their survival and function to achieve the desired clinical outcome.

Bone morphogenetic protein-2 (BMP-2) is a potent osteoinductive molecule that induces osteogenic differentiation of responsive cells and stimulates bone healing and fracture repair.[13–16] However, the supraphysiological dosages required to achieve bone growth in human patients have been linked to ectopic bone formation and prolonged inflammation, increasing potential complications and treatment costs. Furthermore, BMP-2 has been implicated in apoptosis during short-term culture of osteoblasts and MSCs in vitro,[17–19] a challenge that must be resolved in order to promote the efficacy of cell-based therapies. We recently reported that human MSCs induced in osteogenic media exhibited reduced apoptosis in vitro and improved in vivo survival compared to

undifferentiated MSCs.[11] However, it is unknown if MSCs stimulated by BMP-2 for osteogenic differentiation exhibit the same potential.

Localized delivery of BMP-2 with MSCs using effective carrier technologies is an exciting strategy to capitalize on the efficacy of BMP-2 using lower dosages.[20,21] Among the host of biomaterials available, alginate hydrogels are particularly promising for use in biomedical applications as cell carriers and drug delivery vehicles. These materials offer tremendous advantages for bone tissue engineering applications due to their tunable degradation rates and low inflammatory profile, while their mechanical rigidity and degradation rate can be controlled to enhance bone formation.[22,23] Additionally, their cell adhesive properties can be modulated by covalently coupling cell adhesion ligands, such as the arginine–glycine–aspartic acid (RGD) amino acid sequence, to the polymer backbone.[24,25] Recently, photocrosslinked alginate hydrogels (PAHs) have emerged as a promising platform for use in tissue engineering applications,[26–29] as they provide improved control over the degradation rate of the carrier following cross-linking with UV light. However, the efficacy of this platform as a carrier of osteogenic factors has not been examined in an orthotopic bone defect.

We hypothesized that the delivery of human MSCs and BMP-2 from a PAH would increase cell persistence by reducing apoptosis, with a secondary hypothesis that the combination of MSCs and BMP-2 in PAHs will effectively promote improved bone repair compared to MSCs in PAHs alone. To test this hypothesis, we entrapped human MSCs in RGD-modified PAHs containing recombinant human BMP-2. The efficacy of this strategy to promote cell survival and bone regeneration was evaluated both in vitro and in vivo.

2. Results

2.1. PAH Synthesis and BMP-2 Release Kinetics

Figure 1A illustrates the method to fabricate MSC-laden PAHs, some containing BMP-2. After mixing the constituents, macromer solution was placed between quartz plates or in glass tubes and irradiated with 365 nm UV light for 30 min. The resulting PAHs (Figure 1B) are sufficiently robust to facilitate handling and culture for more than 2 weeks.[29] We subsequently measured the release of BMP-2 from PAHs in vitro. We observed a burst of BMP-2 released over the first 2 d, after which release was much slower and sustained (Figure 1C). After 14 d of elution, ≈60% of the initial BMP-2 remained in the PAH. We tested the bioactivity of eluted BMP-2 using MC3T3-E1 murine preosteoblasts, a cell line responsive to BMP-2 stimulation over a range of dosages. The eluted BMP-2 retained its activity, exhibited by its potential to induce intracellular alkaline phosphatase (ALP) activity in MC3T3s at levels comparable to culture media supplemented with fresh BMP-2 (Figure 1D).

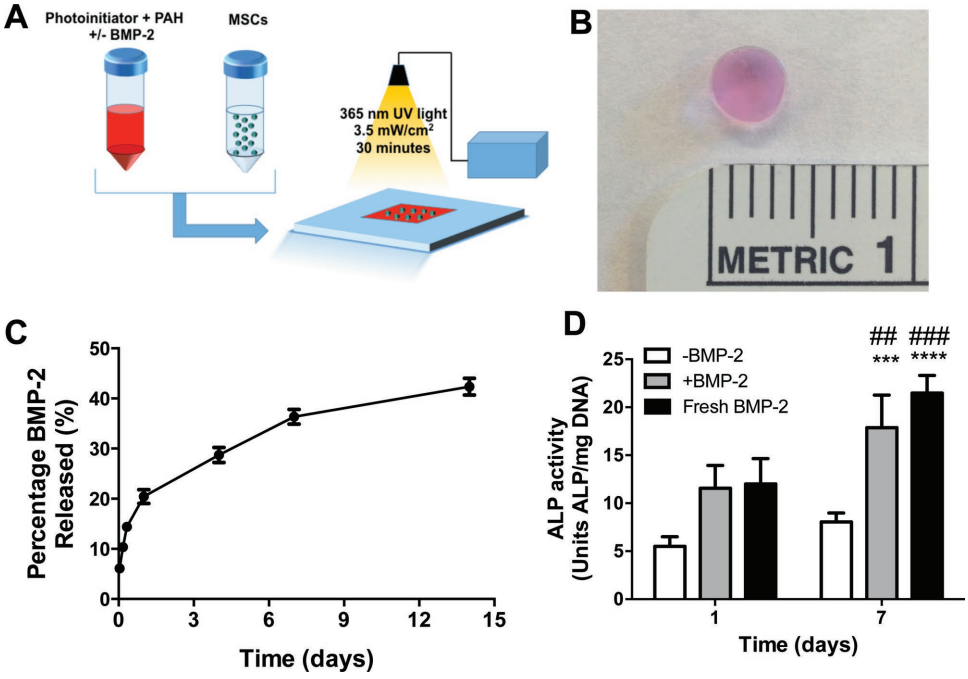

Figure 1. A) Schematic illustrating synthesis of photocrosslinked alginate hydrogels (PAHs) containing MSCs and BMP-2. B) Gross morphological image of representative hydrogel 24 h after synthesis. C) Release kinetics of 2 μg BMP-2 from PAH over 14 d in vitro ($n = 4$). Sustained release of recombinant human BMP-2 was observed during the first week. D) ALP activity in MC3T3-E1 preosteoblasts when stimulated by eluted BMP-2 as demonstration of BMP-2 bioactivity. Positive control is media supplemented with 100 ng mL^{-1} fresh BMP-2; $n = 4$; ***$p < 0.001$, ****$p < 0.0001$ versus –BMP-2 at Day 7; $^{\#\#}p < 0.01$, $^{\#\#\#}p < 0.001$ versus respective Day 1 group.

Adv. Healthcare Mater. 2016,
DOI: 10.1002/adhm.201600461

2.2. BMP-2 Reduces Apoptosis and Promotes MSC Survival In Vitro

We examined the capacity of BMP-2 entrapped in PAHs with MSCs to promote survival under proapoptotic conditions that mimic those observed upon delivery to large bone defects in vivo. We observed similar levels of viable cells by Live/Dead staining after 1 d in serum deprivation and hypoxic (SD/H) conditions in the presence or absence of BMP-2. However, compared to MSCs entrapped in hydrogels lacking BMP-2, we observed a visible increase in the ratio of viable to dead cells after 4 d in SD/H for MSCs entrapped in BMP-2-loaded PAHs (**Figure 2**A). These differences were apparent when quantifying the number of live and dead cells (Figure 2B). We also measured caspase 3/7 activity, an indicator of cell apoptosis, to quantify differences in viability. Caspase activity was lower in MSCs entrapped in BMP-2 loaded hydrogels after 4 d in culture, in agreement with Live/Dead staining (Figure 2C). No significant differences in DNA content were detected between groups over the 4-d study (Figure 2D). We did not detect appreciable differences in cell survival when MSCs were cultured under standard culture conditions, whether in the presence or absence of BMP-2 (data not shown).

2.3. BMP-2 Promotes Osteogenic Differentiation of MSCs Entrapped in PAHs

We analyzed the osteogenic response of MSCs encapsulated in PAHs in the presence or absence of BMP-2 and in the absence of other soluble osteogenic cues, similar to the in vivo environment where the construct would be delivered. We detected an increase in intracellular ALP activity, an early marker of osteogenic differentiation, at both 1 and 7 d when MSCs were entrapped in BMP-2 containing PAHs (**Figure 3**A). MSCs in PAHs lacking BMP-2 exhibited unchanged ALP activity during the same period. MSC secretion of osteocalcin, a later marker of osteogenic differentiation, was significantly higher in hydrogels containing BMP-2 at 7 d of culture (Figure 3B). We also assessed calcium deposition within the PAHs, a late stage marker of osteogenic differentiation. Values for both groups were comparable at 7 d. After 14 d of culture, the calcium content did not change for MSCs in PAHs lacking BMP-2. However, we detected a significant increase in calcium content within hydrogels containing BMP-2 after 14 d in culture (Figure 3C).

2.4. BMP-2 Promotes Survival of MSCs and Resultant Bone Formation In Vivo

A cross-linked PAH containing MSCs was fitted into a clean bone defect, completely filling the defect and residing flush with the defect margins. Using whole body bioluminescence imaging, we detected higher bioluminescence values, suggestive of greater cell survival, for all time points when MSCs were implanted in PAHs containing BMP-2 (**Figure 4**A). As early as 1 week after implantation, there was a strong trend for increased survival of MSCs in the presence of BMP-2. MSCs deployed with BMP-2 exhibited significantly increased cell survival 2 weeks postimplantation (Figure 4B). Conversely, MSCs delivered in hydrogels lacking BMP-2 exhibited a steady decrease in bioluminescent signal over the 4-week study. Compared to values 1 week postimplantation, the bioluminescence intensity was markedly diminished in both groups after 4 weeks.

Codelivery of MSCs and BMP-2 from PAHs decreased fracture healing time and improved tissue mineralization. Using radiography to follow defect closure, we observed improved healing in defects treated with MSCs and BMP-2 as early as 4 weeks (**Figure 5**A). Defects treated with PAHs carrying both MSCs and BMP-2 demonstrated 100% radiographic union at 8 and 12 weeks (Figure 5B). Quantification of tissue volume and bone volume within repair tissue of explants using microCT revealed significantly higher bone volumes at 12 weeks (Figure 5B,C). Defects treated with MSCs alone did not fully bridge and yielded less tissue repair over 12 weeks.

We observed significant increases in matrix deposition in BMP-2-treated defects following histological analysis of explant tissues (**Figure 6**A,B). In agreement with microCT data, we observed the presence of denser tissue in BMP-2 treated defect sites. Additional immunohistochemical analysis revealed extensive deposition of collagen in both defects (Figure 6C,D). Unlike defects treated PAHs loaded with MSCs alone (Figure 6E), positive staining for osteocalcin was extensively observed in defects treated with BMP-2-loaded MSC-laden PAHs (Figure 6F). Taken together with our bioluminescence data revealing loss of human cells ≈4 weeks after implantation, these data suggest that host cells are undergoing osteogenic differentiation.

Increases in bone volume and matrix content detected using radiography, microCT, and histology were confirmed by evaluating the biomechanical properties of repair tissue using torsional testing to failure. Both torsional stiffness (**Figure 7**A) and torque-to-failure (Figure 7B) of defects treated with MSCs and BMP-2 in PAHs were significantly higher than defects treated without BMP-2.

3. Discussion

The combinatorial delivery of osteoinductive growth factors such as BMP-2 with bone-forming progenitor cells is an exciting strategy to promote repair of large bone defects as an alternative to bone grafts. The successful deployment of pharmacological or biological stimuli designed to jumpstart healing requires an appropriate carrier that localizes the material at the target site, protects the payload from premature inactivation, and does not impede native tissue repair processes. MSCs are under broad investigation for their potential to promote bone healing.[30,31] Furthermore, BMP-2 is the active ingredient of at least one commercial product that promotes bone formation by delivering high dosages of BMP-2 from a collagen sponge.[32] BMP-2 has been reported to induce apoptosis in numerous cell types in culture, including osteoblasts and MSCs,[17–19] potentially impeding the success of cell-based therapies for bone healing. As engineered biomaterials enable the use of lower dosages of growth factors by sustained presentation to the target site compared to higher dosages used clinically, the goal of this study was to assess the capacity of MSCs transplanted in

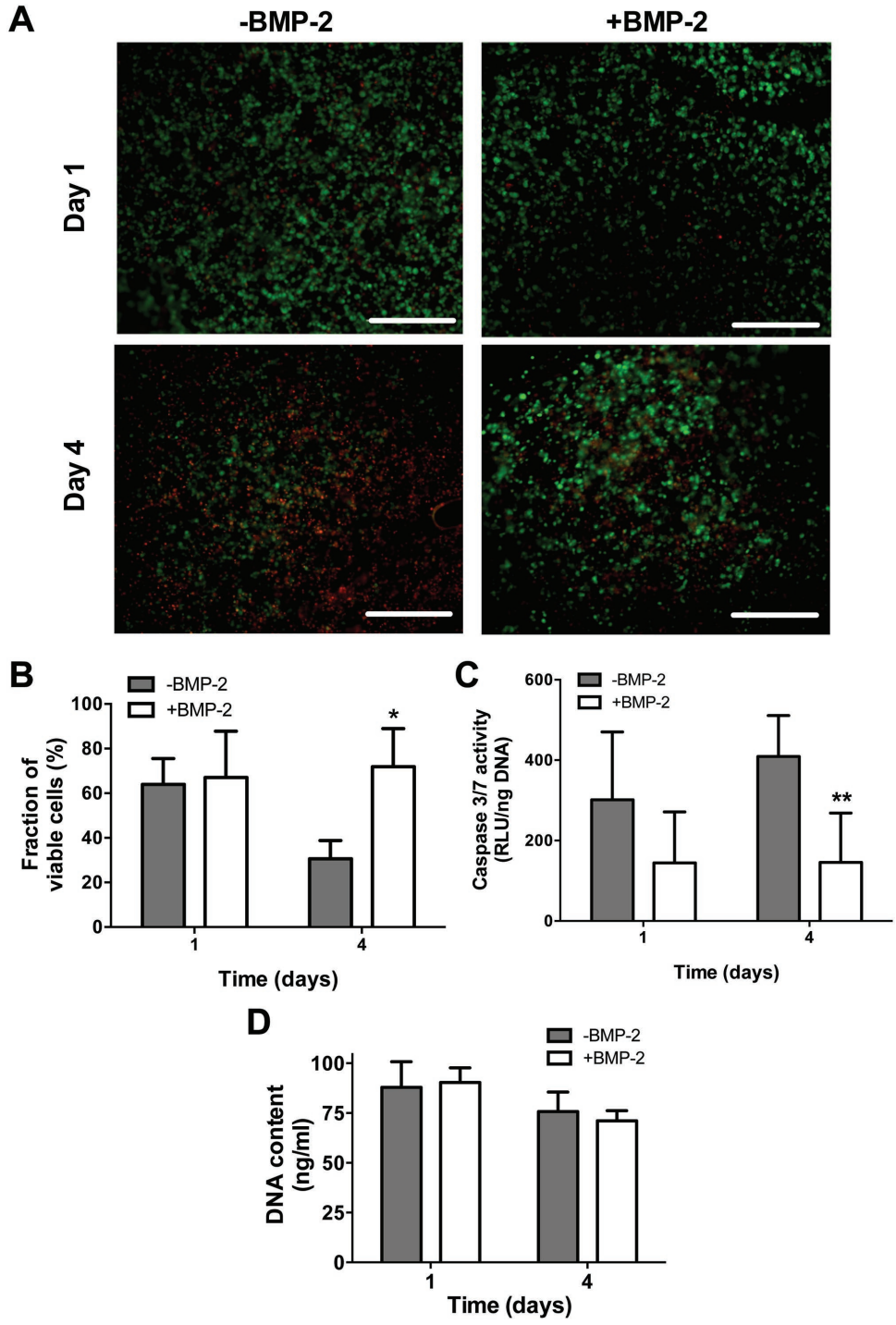

Figure 2. BMP-2 promotes survival of human MSCs entrapped in PAHs under proapoptotic conditions. A) Live/Dead staining of MSCs entrapped in PAHs in the presence or absence of BMP-2 in serum deprivation/hypoxia (SD/H). Live cells are green; dead cells are red. Significant cell death is observed at Day 4 in the absence of BMP-2; images at 10× magnification; scale bar represents 200 μm. B) Quantification of Live/Dead images to determine percentage of viable cells ($n = 4$ per group; $^{*}p < 0.05$ versus −BMP-2 at Day 4). C) Caspase 3/7 activity of MSCs entrapped in SD/H ($n = 4$ per group; $^{**}p < 0.01$ versus −BMP-2 at Day 4). D) DNA content in each condition was not significantly different ($n = 4$ per group).

PAHs loaded with BMP-2 to persist and subsequently enhance bone formation.

Alginate hydrogels are under examination for many tissue engineering applications due to their biocompatibility, tailorable mechanical properties, and tunable degradation rate.[22] Furthermore, alginate has been successfully used as a delivery vehicle for BMP-2 to promote healing of large bone defects similar to the defect used in these studies, although higher doses were

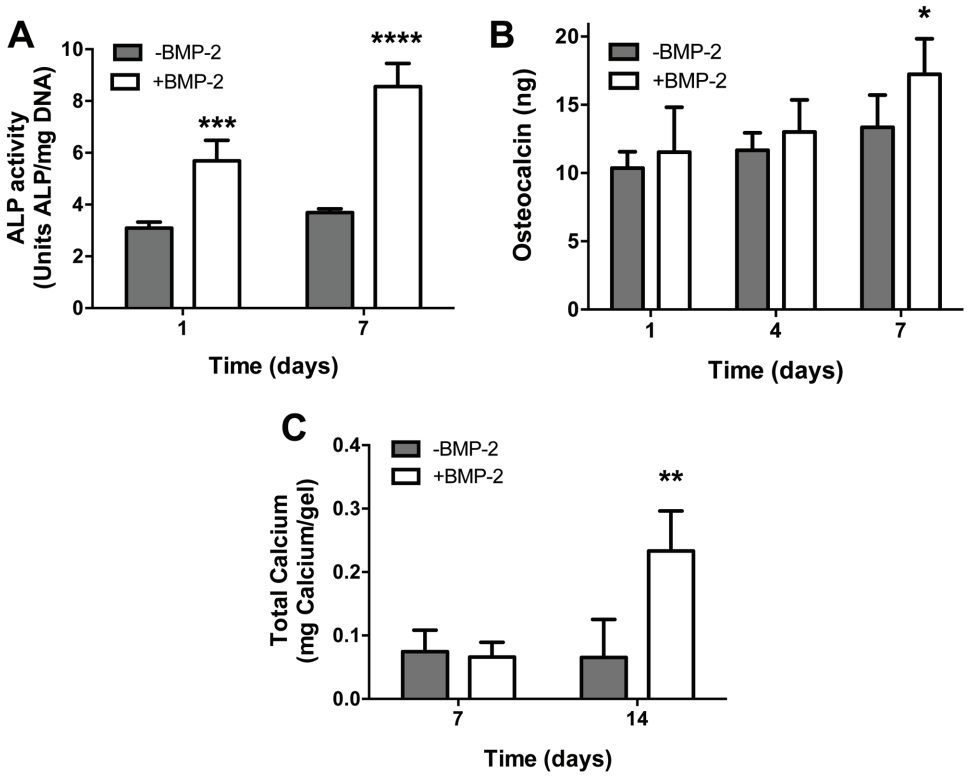

Figure 3. MSCs undergo osteogenic differentiation when entrapped in BMP-2 releasing PAHs. A) ALP activity was higher at 1 and 7 d for MSCs in BMP-2 containing gels (***$p < 0.001$, ****$p < 0.0001$ vs −BMP-2 at the same time point). B) Secreted osteocalcin by MSCs entrapped in alginate gels (*$p < 0.05$ vs −BMP-2 at 7 d). C) Calcium deposition by entrapped MSCs is significantly increased in MSCs entrapped in BMP-2 loaded PAHs (**$p < 0.01$ vs −BMP-2 at 14 d). All data are $n = 4$ per group per time point.

used (5 micrograms).[14] A host of chemistries are available to cross-link alginate hydrogels, with photocrosslinking of this natural polymer offering improved control over degradation by eliminating the material dependence on diffusion of cross-linking cations (i.e., calcium, barium, etc.) and the ionic composition of the surrounding microenvironment.[26,27] Although effective, ionically cross-linked alginate hydrogels have unpredictable degradation rates, and thus the biophysical properties of the implant are difficult to project over the duration of repair. Alternatively, PAH degradation is dependent on the properties of the polymer used to make the hydrogel and not the cross-linking agent, imparting greater control over the temporary extracellular matrix used as a cell carrier and bridge during tissue regeneration. Although not specifically addressed for this study, previous studies report that this PAH formulation loses ≈60% of its mass over 4 weeks.[29] Ideally, the degradation rate of the PAH will be fine-tuned to match the rate of new bone tissue formation by varying, for example, the macromer

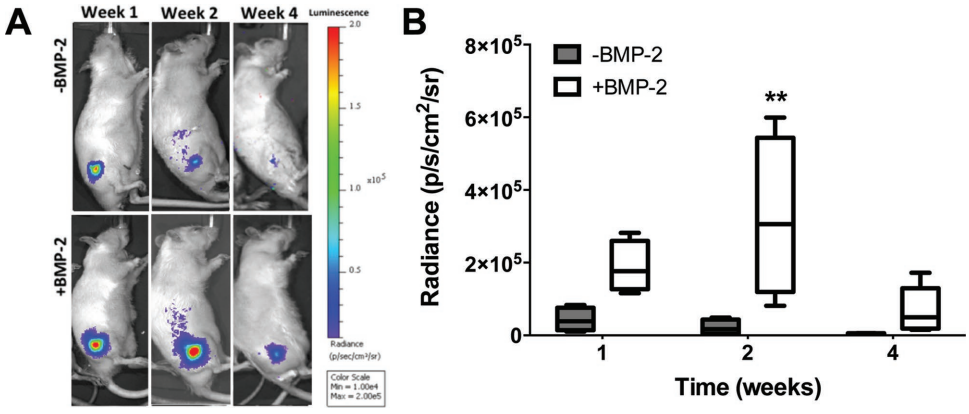

Figure 4. Codelivery of MSCs and BMP-2 in PAHs increased cell persistence in vivo when implanted in a femoral critical-sized defect. A) Representative bioluminescence imaging of the same animal over 4 weeks. B) Quantification of cell signal intensity revealed a significant increase in radiance (an indicator of live cells) in the +BMP-2 group at 2 weeks ($n = 5$ per group; **$p < 0.01$ vs −BMP-2 at 2 weeks).

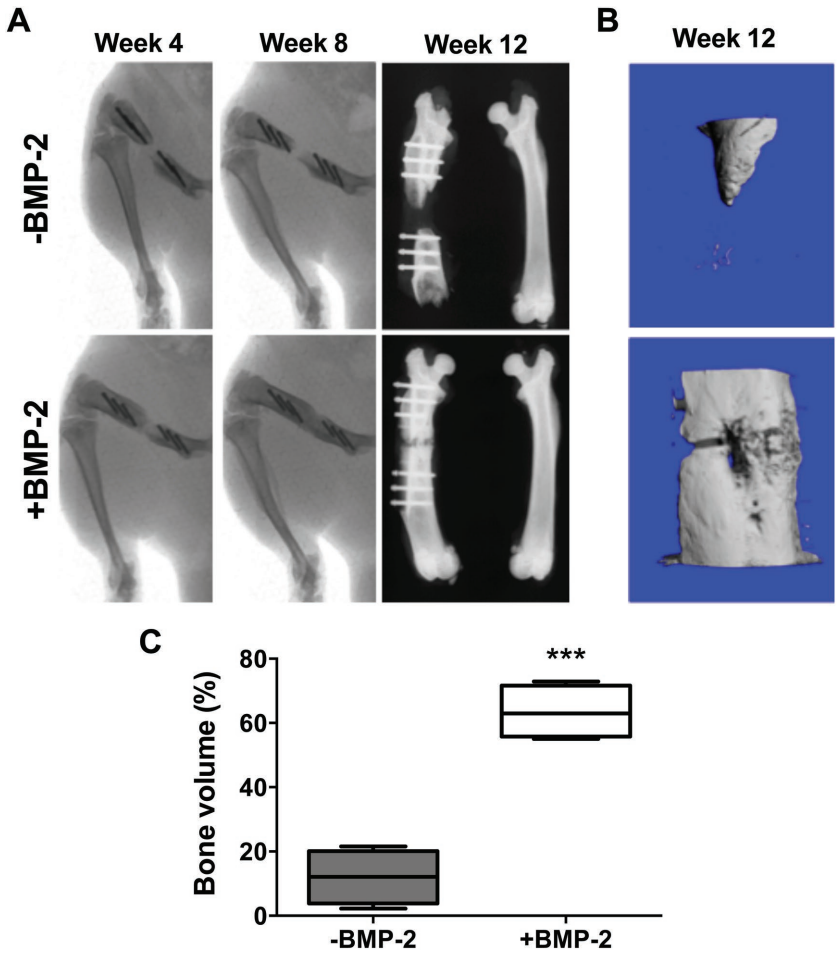

Figure 5. MSCs deployed in BMP-2-loaded PAHs enhanced defect repair compared to MSCs deployed in PAHs without BMP-2. A) Radiographs reveal the presence of increased mineralized tissue within the defect in the +BMP-2 group at 4-, 8-, and 12-weeks postimplantation. Radiographs at 4 and 8 weeks were performed on live animals, while 12-week radiographs were performed on explanted tissue. B) MicroCT scans reveal a significant increase in bone volume within the defect for the +BMP-2 group (bottom) at 12 weeks. C) Bone volume within the original tissue defect is significantly increased in animals treated with BMP-2 at 12 weeks ($n = 6$ for +BMP-2, $n = 4$ for -BMP-2; ***$p < 0.001$ vs −BMP-2).

concentration, the degree of oxidation and/or the degree of methacrylation. The potential to induce gelation of PAHs in situ with light affords increased potential to fill irregularly shaped defects using this temporary extracellular matrix. The efficacy of PAHs as a cell carrier to promote bone healing or deliver inductive factors has been demonstrated in vitro[26–29,33] and in an ectopic bone site,[33] but these studies are the first to confirm its efficacy in a critical-sized orthotopic defect.

Photocrosslinking of alginate hydrogels requires exposure of cells to UV light. Thus, it was critical for us to evaluate cell survival in PAHs containing BMP-2. In these studies, the prolonged presentation of BMP-2 to entrapped MSCs under pro-apoptotic culture conditions resulted in improved cell survival and reductions in apoptosis. Previous data suggest BMP-2 can induce apoptosis in human MSCs following exposure in monolayer culture for a brief period, and the effect was more pronounced as cells become more osteoblastic in maturity.[19] At this time, there is no clear consensus on efficacy of BMP-2 doses to induce MSC osteogenic differentiation in 2D versus 3D culture to compare these data with previous data in monolayer culture. However, we reported that human MSCs induced for 7 d in osteogenic media exhibited significantly reduced caspase activity compared to undifferentiated cells in identical culture conditions used herein.[11] These differences remained when osteoinduced MSCs were implanted in an ectopic site using RGD-modified alginate gels. In this work, we observed a trend for reduced caspase activity in BMP-2-treated MSCs after 1 d. Live/Dead imaging, representing functional impact in cells downstream from caspase activity, did not exhibit differences after 1 d but revealed profound differences after 4 d when caspase activity was significantly different. These data suggest that osteogenically induced MSCs are more robust, resisting apoptosis, and exhibiting improved survival, compared to undifferentiated MSCs.

BMP-2 remained entrapped in PAHs over 14 d in vitro, suggesting that MSCs were continuously exposed to BMP-2 as a protective factor from harsh, proapoptotic conditions that can occur in large bone defects. The high concentration of BMP-2 retained in the alginate is in agreement with previous studies that entrapped BMP-2 in ionically cross-linked alginate hydrogels.[14] Others have reported greater release of BMP-2 when examining elution into phosphate buffered saline (PBS),[33] suggesting the constituents present in the implantation site may impact the concentration of available protein to entrapped or resident host cells.

As expected, BMP-2 stimulated osteogenic differentiation of entrapped MSCs in vitro, even when measured in the absence of other soluble osteogenic cues. Early, intermediate, and late stage markers of osteogenic differentiation were consistently increased in MSCs entrapped in BMP-2 containing PAHs compared to gels lacking BMP-2. These data demonstrate that PAHs containing BMP-2 at doses lower than required to promote effective bridging of this bone defect[34] can initiate the osteogenic program of MSCs without additional soluble osteogenic cues present in lineage specific media.

Upon implantation into a critical-sized femoral bone defect, we observed increased cell survival using noninvasive whole body bioluminescence imaging. MSCs deployed in BMP-2 containing PAHs consistently exhibited higher levels of cell persistence at each time point over 4 weeks. Cell survival peaked at 2 weeks for MSCs deployed with BMP-2, yet persistence was markedly reduced in both groups after 4 weeks. The improved persistence observed with optical imaging is in agreement with previous data from our group demonstrating osteoinduced MSCs exhibit improved survival in vivo compared to undifferentiated cells.[11] Thus, BMP-2 may be acting simultaneously to

Adv. Healthcare Mater. 2016,
DOI: 10.1002/adhm.201600461

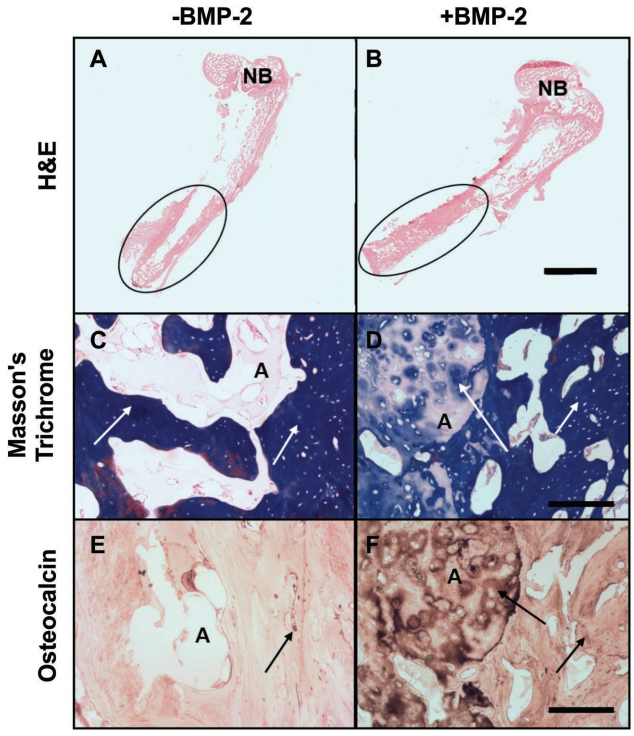

Figure 6. Matrix deposition and bone formation are enhanced in defects containing BMP-2 loaded PAHs compared to PAHs lacking BMP-2. A–B) Representative H&E staining of intact femur. The defect site is indicated by ellipse, representing greater tissue formation in BMP-2 treated defects; scale bar = 4 mm. C–D) Representative Masson's Trichrome staining at 10× magnification; scale bar = 500 μm. E–F) Representative osteocalcin immunohistochemical staining at 10× magnification; scale bar = 500 μm. NB = native bone, A = alginate, white arrows denote matrix deposition, black arrows indicate positive osteocalcin staining.

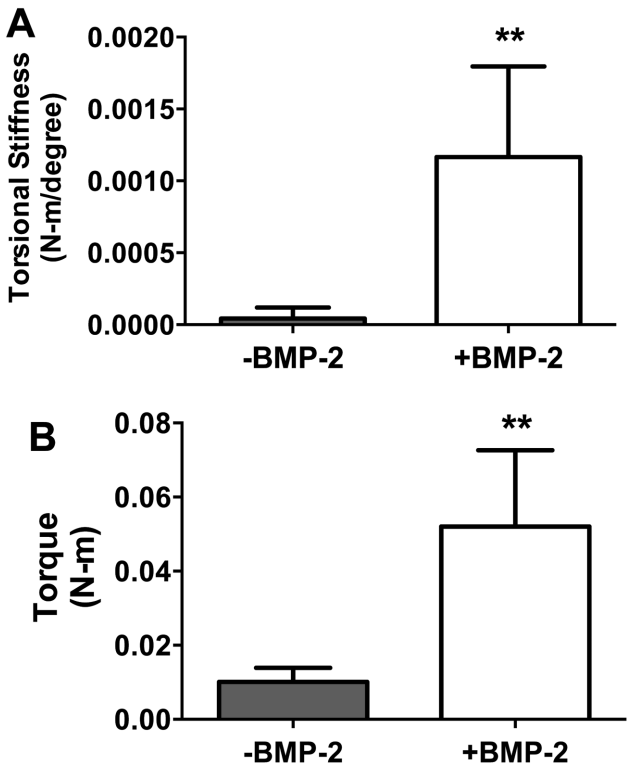

Figure 7. Regenerated bone formed with MSCs transplanted in BMP-2-loaded PAHs exhibits improved mechanical properties compared to defects treated without BMP-2. A) Torsional stiffness and B) torque to failure were each significantly increased for bone defects treated with MSCs in PAHs with BMP-2 (+BMP-2) compared to those defects treated without BMP-2 (n = 4 for +BMP-2, n = 5 for −BMP-2; $^{**}p < 0.01$ vs −BMP-2).

directly protect MSCs from apoptosis through an as yet undetermined pathway, while inducing osteogenic differentiation of cells that imparts greater resistance to cell death. The precise mechanism of action merits further investigation.

We observed significant increases in the rate and quality of bone bridging for defects treated with MSCs in BMP-2 loaded PAHs compared to MSCs alone. Radiography revealed accelerated defect closure in vivo at 4 and 8 weeks. Radiography and microCT 12 weeks posttreatment confirmed that all defects treated with BMP-2 were fused, while no defects treated with MSCs alone attained bridging. Histological analysis and mechanical testing of repair tissue support these data. Furthermore, these data are in agreement with other groups deploying MSCs or BMP-2 from calcium cross-linked alginate into critical-sized bone defects.[14,20] In light of improved cell survival when using BMP-2 at doses lower than commonly employed in rat bone defects,[14,35,36] these findings may enable the use of lower concentrations of MSCs or BMP-2, depending on the availability of cells for treatment.

The purpose of this study was to discern whether low dose BMP-2 could promote MSC survival when entrapped in PAHs. In light of previous studies that demonstrated the capacity of low dose BMP-2 released from ionically cross-linked alginate to promote full healing in this model,[14,37] we did not include this group in our studies because it would not allow us to directly test our hypothesis. However, the absence of this control group represents a limitation of the study, as no conclusions can be made regarding the effects of the delivered MSCs on bone healing. Additional studies are merited to determine the minimum BMP-2 dose necessary to promote survival of MSCs in order to speed bone healing directly or through indirect methods.

4. Conclusion

Engineered PAHs represent a promising delivery vehicle for cellular and protein therapeutics. These findings demonstrate the effective use of PAHs to deliver MSCs and low dose BMP-2 to promote cell survival and bone repair in challenging bone defects. This strategy is easily tailorable by manipulating the dose of entrapped cells and protein, as well as the biophysical properties of the hydrogels.

5. Experimental Section

Cell Culture: Human bone marrow-derived MSCs (Lonza, Walkersville, MD, USA) were expanded under standard conditions (37 °C, 21% O_2, 5% CO_2) until use at passage 5–6 in minimum essential alpha medium (α-MEM; w/L-glutamine, w/o ribo/deoxyribonucleosides, Invitrogen,

Waltham, MA, USA) supplemented with 10% fetal bovine serum (Atlanta Biologicals, Atlanta, GA, USA), and 1% penicillin (10 000 U mL^{-1}) and streptomycin (10 mg mL^{-1}) (P/S; Mediatech, Manassas, VA, USA). For in vivo studies, MSCs genetically modified to express firefly luciferase (UC Davis Center of Excellence in Gene Therapy) were expanded in α-MEM and used at passages 9–10.[10] Culture media was refreshed every 3 d.

Human MSC Encapsulation in PAHs: The photocrosslinkable alginate macromers were synthesized as previously described.[26,27,29] The resulting product was composed of oxidized (14%) sodium alginate (4% w/v in α-MEM; Protanal LF 20/40 1 96 000 g mol^{-1}; FMC Biopolymer, Philadelphia, PA, USA), modified with methacrylate side chains (20% degree of modification) to enable photocrosslinking and the RGD peptide sequence (GRGDSP, Commonwealth Biotechnologies, Richmond, VA, USA) to promote cell adhesion. This material has been reported to lose ≈60% of its mass over 4 weeks.[29] Human MSCs (10×10^6 cells mL^{-1}) were suspended in the macromer solution in the absence or presence of human recombinant BMP-2 (2 µg mL^{-1}, Medtronic, Minneapolis, MN, USA).

For in vitro experiments, 800 µL of solution was pipetted into a sterile silicon mold ($21 \times 21 \times 1.5$ mm) overlaid on a sterile quartz plate and a second sterile quartz plate was placed on top. The macromer solution was photocrosslinked (0.05% w/v photoinitiator; Irgacure-2959; Sigma, St. Louis, MO, USA) with 365 nm UV light at ≈3.5 mW cm^{-2} for 15 min (Figure 1).[26,27] After 15 min the plates were flipped and photocrosslinked for an additional 15 min, and 75 µL hydrogels were cut using a sterile 8 mm biopsy punch. To fabricate MSC/hydrogel constructs for in vivo studies, 150 µL of PAH solution carrying 20×10^6 cells mL^{-1} and either 0 or 2 µg BMP-2 per hydrogel was pipetted into a sterile 2.5 mm diameter borosilicate glass tube and photocrosslinked with 365 nm UV light at ≈3.5 mW cm^{-2} for 15 min. Glass tubes were carefully rotated 180° and photocrosslinked for an additional 15 min. The MSC/hydrogel constructs were gently forced from the tube using a glass Pasteur pipette, placed in 500 µL of α-MEM, and allowed to swell overnight in standard culture conditions.

Assessment of BMP-2 Release In Vitro: PAHs (150 µL) loaded with 2 µg BMP-2 were incubated at 37 °C on an XYZ shaker (Stovall, Cole-Parmer, Vernon Hills, IL, USA). At predetermined time points, 500 µL of serum-containing complete media was collected and replaced, and the eluent was frozen until analysis. BMP-2 eluted from each PAH was quantified with a human specific BMP-2 Quantikine ELISA Kit (R&D Systems, Minneapolis, MN, USA) according to the manufacturer's instructions.

Analysis of Bioactivity of Released BMP-2: Following quantification of BMP-2 in the eluent media *via* enzyme linked immunosorbent assay (ELISA), conditioned media was diluted to 100 ng mL^{-1} BMP-2 in Dulbecco's Modified Eagle's Medium (DMEM, Invitrogen). MC3T3-E1 murine preosteoblasts (ATCC, Manassas, VA, USA) were seeded in 12-well culture plates at 50 000 cells cm^{-2} and cultured with DMEM supplemented with or lacking BMP-2. Fresh BMP-2 (100 ng mL^{-1}) served as the positive control. Cells were cultured for 7 d, and bioactivity was assessed by quantifying intracellular ALP activity with a *p*-nitrophenyl phosphate assay.[6,11,38]

Characterization of MSC Survival in PAHs: MSC-laden PAHs were incubated for 24 h at 37 °C in α-MEM under standard culture conditions on an XYZ shaker. Media was refreshed with complete media and cultured for up to 4 d in standard culture conditions. MSC survival in PAHs was also measured when cultured under proapoptotic conditions (serum deprivation/hypoxia, SD/H).[11] For these studies, media was refreshed with serum-free growth media supplemented with 0.1% (w/v) fatty-acid free BSA (Sigma), and MSC/hydrogel constructs were incubated for up to 4 d in Heracell 150i tri-gas incubators (Thermo Scientific) at 1% oxygen. Apoptosis was measured from lysates of MSC/hydrogel constructs collected in passive lysis buffer and quantified using the Caspase-Glo 3/7 Luminescence assay (Promega, Madison, WI, USA) as described.[11,39] Total DNA present in the MSC/hydrogel constructs was determined with a Quant-iT PicoGreen dsDNA kit (Invitrogen) according to the manufacturer's instructions.[11,25] Cell persistence were imaged and characterized with a Live/Dead stain. Briefly, calcein AM and propidium iodide (both from Invitrogen) were added to α-MEM to create a 2×10^{-3} and 5×10^{-3} M reagent solution, respectively. MSC/hydrogel constructs were fully immersed in 500 µL of combined reagent solution, incubated in the dark for 30 min, and imaged with an Olympus Fluoview FV1000 system. Images were quantified for percent cell viability using ImageJ software. Osteogenic potential was assessed at 1, 7, and 14 d by quantifying ALP, osteocalcin secretion with a human osteocalcin Quantikine ELISA according to the manufacturer's instructions, and calcium deposition with an *o*-cresolphthalein assay.[6,11,38]

Rat Femoral Segmental Defect Model of Bone Healing: Animals were treated in accordance with all University of California, Davis animal care guidelines and National Institutes of Health (NIH) animal handling procedures. Male athymic rats (NIH/RNU, 10–12 weeks old, Taconic) were anesthetized and maintained under a 3%–4% isoflurane/O_2 mixture delivered through a nose cone. Six millimeter diaphyseal critical-size defects were created in the right femora of each animal and stabilized with a radiolucent polyetheretherketone plate and six angular stable bicortical titanium screws (RISystem AG, Davos, Switzerland) as described.[40] Defects were immediately filled with MSC/hydrogel constructs containing 0 or 2 µg BMP-2. The incision was closed with suture and buprenorphine (0.05 mg kg^{-1}) was administered twice per day for two days as analgesia.

Assessment of Cell Survival In Vivo: At 1, 2, and 4 weeks, animals were given an intraperitoneal injection of D-Luciferin Firefly (Caliper, Perkin Elmer, Waltham, MA, USA) in sterile PBS (10 µg g^{-1} body weight). All animals were scanned with an IVIS Spectrum (Perkin Elmer), and cell persistence was measured with Living Image software (Perkin Elmer).[11,41] Total photons per second per square centimeter were recorded from each bioluminescent region of interest.

Contact high-resolution radiographs (20 kVp, 3 mA, 2 min exposure time, 61 cm source-film distance) were taken in a cabinet radiograph unit (Faxitron 43805N, Field Emission Corporation, Tucson, AZ, USA) using high-resolution mammography film (Oncology Film PPL-2, Kodak, Rochester, NY, USA), and digitized using a high-resolution flatbed scanner (SilverFast 500 ppi, LaserSoft, Sarasota, FL, USA). Radiographs were obtained at 4, 8, and 12 weeks, and scored by a blinded observer.

All animals were euthanized by CO_2 inhalation at 12 weeks postsurgery. Both femurs were explanted, wrapped in sterile gauze, submerged in PBS, and stored at –20 °C. Excised femurs were imaged (45 kVp, 177 µA, 400 µs integration time, average of four images) using a high-resolution microCT specimen scanner (µCT 35; Scanco Medical, Brüttisellen, Switzerland). Approximately 696 contiguous slices of 2048×2048 pixels were imaged with 6 µm resolution and slice thickness (voxels). Serial tomograms were reconstructed from raw data of 1000 projections per 180° using an adapted cone beam-filtered back projection algorithm. The tomograms were calibrated to a range of concentrations of HA 0.0, 99.6, 200.0, 401.0, and 800.3 mg HA^{-3} in order to convert grey-values (X-ray attenuation) of the images to units of density in mg HA cc^{-1}. A threshold (282–3000 mg HA^{-3}) was determined subjectively from the reconstructed images to partition mineralized tissue from fluid and soft-tissues. After thresholding, the image noise was reduced using a low-pass Gaussian filter ($\sigma = 0.8$, support = 1). A circular region of 0.83 cm^2 was centered on the hydrogel cross-section to create a cylindrical volume. The length of the cylinder was created large enough to surround each individual PAH implanted in the defect site. Bone volume of repair tissue was determined using the accompanying software.

Evaluation of Mechanical Properties of Repair Tissue: Femurs from +BMP- and –BMP-treated animals were harvested after 12 weeks. Femurs were potted between two aluminum blocks with Wood's metal (McMaster-Carr, Cleveland, OH). Femurs were secured in a Bose Electroforce 3200 with associated torsion motor (TA Instruments, New Castle, DE) with an effective testing length of 20 mm. Preloading was performed with ten cycles with a triangle wave to a target rotation of ±5° at 0.1 Hz. Torsional test to failure was performed such that the femoral head was externally rotated at 1° per second until fracture or complete 90° rotation. Time, position, and torque data were recorded at 50 Hz, and torsional stiffness (N-m $degree^{-1}$) and ultimate torque (N-m) were calculated.

Histological Analysis of Repair Tissue: Explants were demineralized in Calci-Clear Rapid (National Diagnostics, Atlanta, GA), processed, paraffin embedded, and sectioned at 5 μm thickness. Sections were stained with hematoxylin and eosin (H&E) and Masson's Trichrome and imaged using a Nikon Eclipse TE2000U microscope and Andor Zyla 5.5 sCMOS digital camera. In order to visualize cells undergoing osteogenic differentiation, immunohistochemistry was performed on sections using a primary antibody against osteocalcin (1:200, ab13420, Abcam, Cambridge, MA)[42,43] and a mouse specific HRP/DAB detection kit (ab64259, Abcam).

Statistical Analysis: Data are presented as means ± standard deviation unless otherwise stated. Statistical analyses were performed with standard *t*-tests with a Welch's correction or one- or two-way ANOVA, followed by a Tukey's or Bonferroni's multiple comparison post hoc test (GraphPad Prism 6.0) when appropriate to assess significance ($p < 0.05$).

Acknowledgements

S.S.H. and N.L.V. contributed equally to this work. This work was supported in part by the Department of the Army W81XWH-10-1-0956 (JKL), NIAMS R01AR066193 (EA), T32 AI060555 (SH), and T32AR007505 (OJ). The authors recognize surgical assistance from Joel Williams, MD, and Hyoung-Keun Oh, MD. The authors appreciate technical assistance from Blaine Christiansen for torsional testing of rat femurs. The authors acknowledge Tanya Garcia-Nolan, Chrisoula Toupadakis Skouritakis, Jennifer Fung, and Charles Smith for assistance in obtaining radiographs and microCT data.

Received: April 25, 2016
Revised: July 13, 2016
Published online:

[1] S. Zwingenberger, C. Nich, R. D. Valladares, Z. Y. Yao, M. Stiehler, S. B. Goodman, *Biodrugs* **2012**, *26*, 245.
[2] G. M. Calori, M. Colombo, E. L. Mazza, S. Mazzola, E. Malagoli, G. V. Mineo, *Injury* **2014**, *45*, S116.
[3] E. Gomez-Barrena, P. Rosset, D. Lozano, J. Stanovici, C. Ermthaller, F. Gerbhard, *Bone* **2015**, *70*, 93.
[4] C. Wen, H. Kang, Y. R. Shih, Y. Hwang, S. Varghese, *Drug Delivery Transl. Res.* **2016**, *6*, 121.
[5] S. Song, E. J. Kim, C. S. Bahney, T. Miclau, R. Marcucio, S. Roy, *Acta Biomater.* **2015**, *18*, 100.
[6] K. C. Murphy, M. L. Hughbanks, B. Y. Binder, C. B. Vissers, J. K. Leach, *Ann. Biomed. Eng.* **2015**, *43*, 2010.
[7] E. Seebach, H. Freischmidt, J. Holschbach, J. Fellenberg, W. Richter, *Acta Biomater.* **2014**, *10*, 4730.
[8] J. He, D. C. Genetos, J. K. Leach, *Tissue Eng. Part A* **2010**, *16*, 127.
[9] G. Ren, X. Chen, F. Dong, W. Li, X. Ren, Y. Zhang, Y. Shi, *Stem Cells Transl. Med.* **2012**, *1*, 51.
[10] A. I. Hoch, V. Mittal, D. Mitra, N. Vollmer, C. A. Zikry, J. K. Leach, *Biomaterials* **2016**, *74*, 178.
[11] B. Y. Binder, D. C. Genetos, J. K. Leach, *Tissue Eng. Part A* **2014**, *20*, 1156.
[12] A. Chatterjea, G. Meijer, C. van Blitterswijk, J. de Boer, *Stem Cells Int.* **2010**, *2010*, 215625.
[13] A. C. Carreira, F. H. Lojudice, E. Halcsik, R. D. Navarro, M. C. Sogayar, J. M. Granjeiro, *J. Dent. Res.* **2014**, *93*, 335.
[14] Y. M. Kolambkar, K. M. Dupont, J. D. Boerckel, N. Huebsch, D. J. Mooney, D. W. Hutmacher, R. E. Guldberg, *Biomaterials* **2011**, *32*, 65.
[15] A. Shekaran, J. R. Garcia, A. Y. Clark, T. E. Kavanaugh, A. S. Lin, R. E. Guldberg, A. J. Garcia, *Biomaterials* **2014**, *35*, 5453.
[16] H. E. Davis, E. M. Case, S. L. Miller, D. C. Genetos, J. K. Leach, *Biotechnol. Bioeng.* **2011**, *108*, 2727.
[17] E. Hay, J. Lemonnier, O. Fromigue, P. J. Marie, *J. Biol. Chem.* **2001**, *276*, 29028.
[18] U. Noth, R. Tuli, R. Seghatoleslami, M. Howard, A. Shah, D. J. Hall, N. J. Hickok, R. S. Tuan, *Exp. Cell Res.* **2003**, *291*, 201.
[19] S. L. Hyzy, R. Olivares-Navarrete, Z. Schwartz, B. D. Boyan, *J. Cell Biochem.* **2012**, *113*, 3236.
[20] C. R. Dosier, B. A. Uhrig, N. J. Willett, L. Krishnan, M. T. Li, H. Y. Stevens, Z. Schwartz, B. D. Boyan, R. E. Guldberg, *Tissue Eng. Part A* **2015**, *21*, 156.
[21] J. Kim, I. S. Kim, T. H. Cho, K. B. Lee, S. J. Hwang, G. Tae, I. Noh, S. H. Lee, Y. Park, K. Sun, *Biomaterials* **2007**, *28*, 1830.
[22] K. Y. Lee, D. J. Mooney, *Prog. Polym. Sci.* **2012**, *37*, 106.
[23] C. J. Kearney, D. J. Mooney, *Nat. Mater.* **2013**, *12*, 1004.
[24] U. Hersel, C. Dahmen, H. Kessler, *Biomaterials* **2003**, *24*, 4385.
[25] A. Bhat, A. I. Hoch, M. L. Decaris, J. K. Leach, *FASEB J.* **2013**, *27*, 4844.
[26] O. Jeon, K. H. Bouhadir, J. M. Mansour, E. Alsberg, *Biomaterials* **2009**, *30*, 2724.
[27] O. Jeon, C. Powell, S. M. Ahmed, E. Alsberg, *Tissue Eng. Part A* **2010**, *16*, 2915.
[28] O. Jeon, E. Alsberg, *Tissue Eng. Part A* **2013**, *19*, 1424.
[29] O. Jeon, D. S. Alt, S. M. Ahmed, E. Alsberg, *Biomaterials* **2012**, *33*, 3503.
[30] A. I. Hoch, J. K. Leach, *Stem Cells Transl. Med.* **2014**, *3*, 643.
[31] W. L. Grayson, B. A. Bunnell, E. Martin, T. Frazier, B. P. Hung, J. M. Gimble, *Nat. Rev. Endocrinol.* **2015**, *11*, 140.
[32] K. D. Hankenson, K. Gagne, M. Shaughnessy, *Adv. Drug Delivery Rev.* **2015**, *94*, 3.
[33] O. Jeon, C. Powell, L. D. Solorio, M. D. Krebs, E. Alsberg, *J. Controlled Release* **2011**, *153*, 258.
[34] A. W. Yasko, J. M. Lane, E. J. Fellinger, V. Rosen, J. M. Wozney, E. A. Wang, *J. Bone Joint Surg. Am.* **1992**, *74*, 659.
[35] J. D. Skelly, J. Lange, T. M. Filion, X. Li, D. C. Ayers, J. Song, *Clin. Orthop. Relat. Res.* **2014**, *472*, 4015.
[36] T. Diab, E. M. Pritchard, B. A. Uhrig, J. D. Boerckel, D. L. Kaplan, R. E. Guldberg, *J. Mech. Behav. Biomed. Mater.* **2012**, *11*, 123.
[37] A. B. Allen, J. A. Zimmermann, O. A. Burnsed, D. C. Yakubovich, H. Y. Stevens, Z. Gazit, T. C. McDevitt, R. E. Guldberg, *J. Mater. Chem. B* **2016**, *4*, 3594.
[38] C. A. B. Vissers, J. N. Harvestine, J. K. Leach, *J. Mater. Chem. B* **2015**, *3*, 8650.
[39] S. Jose, M. L. Hughbanks, B. Y. Binder, G. C. Ingavle, J. K. Leach, *Acta Biomater.* **2014**, *10*, 1955.
[40] J. C. Williams, S. Maitra, M. J. Anderson, B. A. Christiansen, A. H. Reddi, M. A. Lee, *J. Orthop. Trauma* **2015**, *29*, e336.
[41] J. He, M. L. Decaris, J. K. Leach, *Tissue Eng. Part A* **2012**, *18*, 1520.
[42] Y. R. Shih, Y. Hwang, A. Phadke, H. Kang, N. S. Hwang, E. J. Caro, S. Nguyen, M. Siu, E. A. Theodorakis, N. C. Gianneschi, K. S. Vecchio, S. Chien, O. K. Lee, S. Varghese, *Proc. Natl. Acad. Sci. USA* **2014**, *111*, 990.
[43] S. S. Ho, K. C. Murphy, B. Y. Binder, C. B. Vissers, J. K. Leach, *Stem Cells Transl. Med.* **2016**, *5*, 773.